Наносистеми, наноматеріали, нанотехнології
Nanosistemi, Nanomateriali, Nanotehnologii
2023, т. 21, № 1, сс. 87–98

PACS numbers: 78.67.-n, 81.07.Pr, 81.40.Tv, 84.60.Jt, 85.60.Bt, 88.40.H-

Simulation Analysis of Formamidinium Lead Iodide Perovskite Solar Cells as Function of Thickness and Defects of Absorber Layer, Hole and Electron Transport Layer Under SCAPS-1*D*

Ourida Ourahmoun

Electronic Department,
LATAGE Laboratory,
Faculty of Electrical Engineering and Computing,
University of Mouloud Mammeri of Tizi-Ouzou,
15000 Algeria

This paper reports the simulation and optimization of the perovskite-based photovoltaic solar cell. The basic perovskite solar cell simulated in this work is a planar *n*–*i*–*p* structure. It consists of three different layers: a perovskite absorbing layer, which is sandwiched between the electron-transport layer (ETL) and the hole-transport layer (HTL). The present paper shows numerical simulations of a planar heterojunction solar cell having the following structure: FTO/ETL/perovskite/HTL/Au (FTO—fluorine-doped tin oxide). Formamidinium lead triiodide ($FAPbI_3$) is used as perovskite absorber material; intrinsic tin oxide (*i*-SnO_2) and tungsten disulphide (WS_2) are used as electron-transport layer, and cuprous oxide (Cu_2O) and Spiro-OMeTAD are used as hole-transport layer. The effects of the ETL and HTL types and the thickness of each layer are given by means of simulation using SCAPS-1*D* software. The obtained results show that a cell with WS_2 (50 nm), $FAPbI_3$ (750 nm) and Cu_2O (10 nm) gives better efficiency of 26.07%.

У даній статті повідомляється про моделювання й оптимізацію фотоелектричного сонячного елемента на основі перовськіту. Основним перовськітним сонячним елементом, змодельованим у цій роботі, є пласка *n*–*i*–*p*-структура. Він складається з трьох різних шарів: перовськітного вбирного шару, який затиснутий між електронно-транспортним шаром (ETL) і дірковим транспортним шаром (HTL). Наведено чисельне моделювання плаского гетероперехідного сонячного елемента з наступною структурою: FTO/ETL/перовськіт/HTL/Au (FTO — оксид Стануму, леґований Фтором). Трийодистий Плюмбум–формамідин ($FAPbI_3$) використовується як матеріял-вбирач перовськіту; власний оксид Стануму (*i*-SnO_2) і дисульфід Вольфраму (WS_2) використовуються в якості електронно-транспортного шару, а оксид Купруму (Cu_2O) і Spiro-

OMeTAD використовуються в якості діркового транспортного шару. Ефекти ETL- і HTL-типів і товщина кожного шару задаються за допомогою моделювання із використанням програмного забезпечення SCAPS-1*D*. Одержані результати показують, що комірка з WS_2 (50 нм), $FAPbI_3$ (750 нм) і Cu_2O (10 нм) дає ліпшу ефективність у 26,07%.

Key words: perovskite solar cells, SCAPS-1*D* simulation, electron-transport layer, cuprous oxide, tungsten disulphide, defects.

Ключові слова: перовськітні сонячні елементи, моделювання SCAPS-1*D*, електронно-транспортний шар, оксид Купруму, дисульфід Вольфраму, дефекти.

(Received 27 July, 2022)

1. INTRODUCTION

Perovskite based solar cells have great photovoltaic performance with power conversion in a wide region of optical absorption [1]. However, the simplicity and ease of device fabrication from solution with the realization of efficiencies > 21% made serious claims for commercialization as future photovoltaic technology [2].

The perovskite solar cells consists of titanium oxides as an electron transporting layer, perovskite crystal as a photoactive layer and 2,2′, 7,7′-tetrakis-(N, N-di-4-methoxyphenylamino)-9, 9′-spirobifluorene (Spiro-OMeTAD) as a hole transporting layer (HTL) [3, 4]. The chemical structures of perovskite materials are $MAPbX_3$ and $FAPbX_3$ varied with mole ratio of halogen anions (X = iodine:I, bromine:Br, chlorine:Cl). Hybrid organometal trihalide perovskites ($MAPbX_3$, X = Cl, Br or I) have recently emerged as a promising candidate for photovoltaic application. This is due to the excellent photoelectric properties and facile solution processing such as a direct band gap of 1.55 eV, absorption coefficient of above 10^4 cm^{-1}, a weak binding energy of about 0.03 eV, and an impressively low difference between open-circuit voltage (V_{OC}) and its band gap potential.

The performance of the perovskite solar cells depends on the absorber layer, the electron-transport layer (ETL), the hole-transport layer (HTL) and electrodes. Various structures and architectures are studied. Improving the performance of perovskite solar cells requires the development of new materials, optimization of cell structure and associated manufacturing technology. Organic and inorganic materials are used as interfacial layers. The use of inorganic materials as hole-transport layer (HTL) such as Cu_2O, CuI, V_2O_5, MoO_3, CdS, and NIO, and electron-transport layer (ETL) such as TiO_2, SnO_2, WS_2 [5], ZnSe, CuSCN [6], CuSeCN and ZnO, improves the stability of the cells. Doping the HTL improves the electrical

properties of the layer and then enhances the efficiency; also, the use of a protective layer between HTL and the anode of the cell enhances the yield. The use of carbon contacts improves the stability of the cell. Organic materials are also used as interfacial layers, Pedot:Pss, Spiro-OMeTAD and P_3HT are used as HTL, ICBA, $PC_{60}BM$, $PC_{70}BM$ and C_{70} are used as ETL. The power conversion efficiency of perovskite solar cells with $PC_{70}BM/C_{70}$ dual ETLs and Pedot:Pss/PTB7 dual HTLs were improved [7].

Perovskite materials are sensitive to atmospheric conditions and especially to humidity. To improve performance of photovoltaic cells and protect cells from degradation, an encapsulation is required. The encapsulation is used to protect the cells against the penetration of O_2 and H_2O into the cells and to improve their efficiency and stability [8, 9]. To protect cells against moisture, inorganic layers are used as HTL or ETL.

The toxicity of lead used in the absorber layer is another disadvantage of these devices. To improve environmental impact, lead-free perovskite materials such as $FASnI_3$, $FAGeI_3$, $FACsI_3$ and Cs_2TiX_6 are used as absorber layers [10].

The slight addition of silicon phtalyocianine into the perovskite layer caused suppression of defect and pinhole in the surface layer, which had the best performance. The phtalyocyanine complexes play an important role for improving the crystal growth, carrier generation and diffusion without carrier recombination and trapping near the defect and pinhole in the perovskite layer [11].

Tungsten disulphide (WS_2) is used as an electron transport layer material. WS_2 shows good optoelectronic properties as follows: the band gap in the range of 1.33–2.22 eV, electronic properties can be tuned by doping other atoms or by applying an external force to change its structure, it shows excellent electron-transport capabilities because of high electron mobility [6].

Cuprous oxide (Cu_2O) is characterized as a non-toxic material that is easily available, inexpensive and has a high absorption coefficient in the visible range. Cu_2O have a wide band gap ranging from 2.1 to 2.61 eV [10]. It is type *p* and is used as hole-transport layer.

The performance of the solar cell decreases with increase of metal work function, the majority carrier barrier height increases, thus, efficiency decreases [10].

Device simulation is a strong tool to understand device physics and optimum design for efficiency improvement. In particular, Solar Cell Capacitance Simulator 1-dimensional (SCAPS-1*D*) is a simulation program that calculates energy bands, concentrations and currents, J–V characteristics and spectral response among other device parameters by solving the three basic semiconductor equations (the continuity equations for hole and electrons and Poisson's equa-

tion) under the constraint of boundary conditions. The program has been widely applied to inorganic semiconductor solar cell modelling, such as silicon, CIGS and CdTe solar cells.

In this work, a theoretical study was carried out using SCAPS-1*D* in order to find optimized value that improve future efficiencies of perovskite solar cells. SCAPS-1*D* simulation is used to explain the effect of the variation of the thickness of the absorber layer, hole-transport layer and electron-transport layer in the photovoltaic parameters of the cells. The influence of the defects of the absorber layer used in the structure is presented. The effect of the series resistance is also simulated.

This study optimized perovskite solar cells with an *n*–*i*–*p* configuration using SCAPS-1*D*. Several materials are investigated as HTL or ETL. The absorber layer used is $FAPbI_3$, because studies shows that $FAPbI_3$ exhibits better efficiency compared to other perovskite materials. FTO/WS_2/$FAPbI_3$/Cu_2O/Au (FTO—fluorine-doped tin oxide) have been optimized by numerical computation using SCAPS-1*D* simulation software.

The thickness of each layer is varied and their impact on different performance parameters was deeply explored.

2. ELECTRICAL SIMULATION OF THE PEROVSKITE CELL

2.1. Structure of the Perovskite Cells

The structure of the simulated perovskite solar cells is presented in Fig. 1. The absorber layer $FAPbI_3$ is sandwiched between the hole-transport layer (Spiro-OMeTAD or Cu_2O) and the electron-transport layer (*i*-SnO_2 or WS_2). The objective of this work is to compare the performance of the cells as function of thicknesses of layers and the type of HTL and ETL. SCAPS-1*D* software is used for the simulation.

2.3. Parameters Used in the Simulation

Table illustrates the parameters of each layer used in the simulation. FTO is used as transparent electrode, formamidinium lead iodide ($FAPbI_3$) is the active absorber layer, and Spiro-OMeTAD and Cu_2O are HTLs. Finally, *i*-SnO_2 and WS_2 are used as ETLs.

3. RESULTS AND DISCUSSIONS

3.1. Effect of the Absorber Layer Thickness

When the thickness of the absorber layer ($FAPbI_3$) increases, the

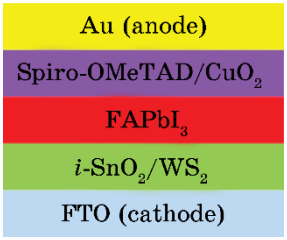

Fig. 1. Structure of the perovskite solar cell simulated under SCAPS-1*D*.

TABLE. Material parameters for different layers used in simulation

Design parameters	FTO	$FAPbI_3$	Spiro-OMeTAD	Cu_2O [12]	*i*-SnO_2 [12]	WS_2 [6]
E_g, eV	3.2	1.51	2.9	2.2	3.6	1.87
Electron affinity, eV	4.4	4	2.2	3.3	4.5	4.3
Dielectric constant	9.2	6.6	3	9	9	11.9
DOS of conduction band, cm^{-3}	$1.1 \cdot 10^{19}$	$1.2 \cdot 10^{19}$	$2.2 \cdot 10^{18}$	$1.8 \cdot 10^{18}$	$2.2\ 10^{18}$	$1 \cdot 10^{18}$
DOS of valence band, cm^{-3}	$1.1 \cdot 10^{19}$	$2.9 \cdot 10^{18}$	$2.2 \cdot 10^{18}$	$2.4 \cdot 10^{19}$	$1.8\ 10^{19}$	$2.4 \cdot 10^{19}$
Thermal velocity of electron V_{the}, cm/s	$1.1 \cdot 10^{7}$	10^{7}	10^{7}	10^{7}	10^{7}	$1.1 \cdot 10^{7}$
Thermal velocity of hole V_{thh}, cm/s	$1.1 \cdot 10^{7}$	10^{7}	10^{7}	10^{7}	10^{7}	$1.1 \cdot 10^{7}$
Uniform donor density N_D, cm^{-3}	$1.2 \cdot 10^{18}$	$1.3 \cdot 10^{16}$	0	0		$1.1 \cdot 10^{19}$
Uniform acceptor density N_A, cm^{-3}	0	$1.3 \cdot 10^{16}$	$1.3 \cdot 10^{18}$	$5 \cdot 10^{18}$	0	0
Mobility of electrons μ_e, cm^2/VS	21	2.7	10^{-4}	200		260
Mobility of holes μ_h, cm^2/VS	11	1.8	10^{-4}	25		51

efficiency increases, and from 750 nm of $FAPbI_3$, the PCE tends to stabilize, and PCE is of the order of 24.18%. Fill factor (FF) decreases as the thickness of $FAPbI_3$ increases as shown in Fig. 2, *a*.

The short-circuit current density J_{SC} increases as the thickness of the absorber layer increases. The open-circuit voltage V_{OC} decreases when the thickness of $FAPbI_3$ increases as shown in Fig. 2.

Figure 2, *c* illustrates the $J(V)$ characteristics as function of the

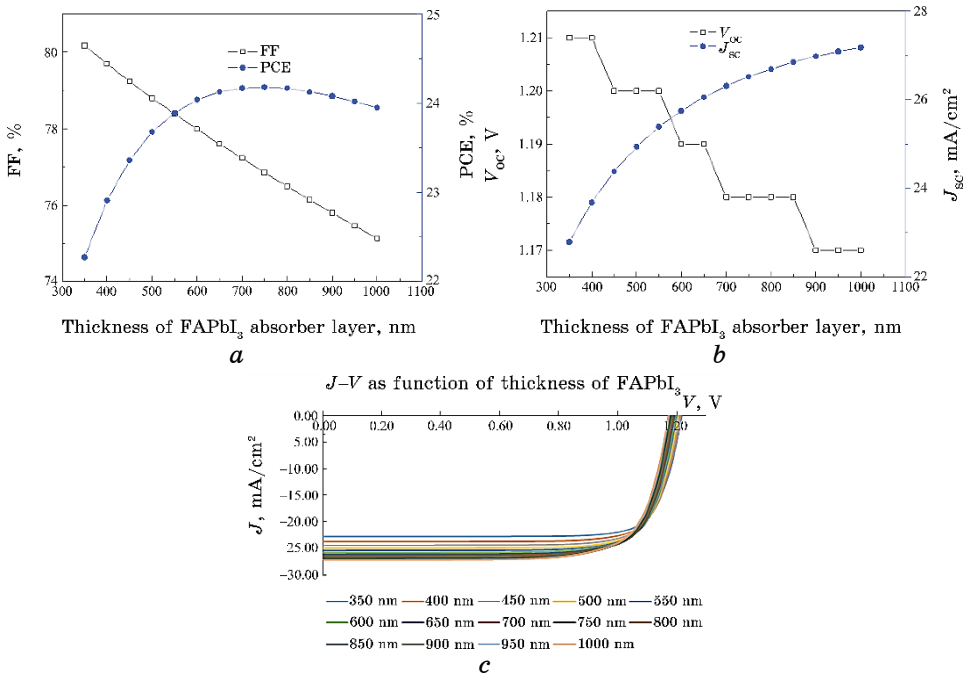

Fig. 2. Simulation of $FAPbI_3$ based perovskite cell as function of the thickness of the absorber layer with SnO_2 (70 nm), Spero-OMeTAD (200 nm). (*a*) Efficiency and fill factor; (*b*) V_{OC} and J_{SC}, (*c*) $J(V)$ characteristics as function of the $FAPbI_3$ thicknesses.

$FAPbI_3$ thicknesses.

3.2. Effect of the Hole Transport Layer Thickness

3.2.1. Effect of the Thickness of Spiro-OMeTAD

Spiro-OMeTAD proved its effectiveness as a hole-transport layer, as its band gap highly matches that of the perovskite materials [13], the perfect conductivity of doped Spiro-OMeTAD [14], and its high melting point, making it preferable choice for many researchers.

Results obtained by simulation show that, when the thickness of the Spiro-OMeTAD used as hole-transport layer increases from 10 nm to 70 nm, the power conversion efficiency and the fill factor decrease as shown in Fig. 3, *a*. The variation of the thickness of Spiro-OMeTAD does not influence the short-circuit current and the open-circuit voltage, $J_{SC} = 26.52$ mA/cm^2 and $V_{OC} = 1.8$ V, as shown in Fig. 3, *b*.

3.2.2. Effect of Cu_2O as Hole-Transport Layer

Cu_2O is used as HTL because of its excellent properties as follow: high optical transparency in visible light spectrum, fast hole-transportation capability as it has hole mobility, prepared using simple solution process with relatively good chemical stability.

A perovskite cell with Cu_2O used as HTL is simulated under SCAPS-1*D*. The thickness of Cu_2O was varied from 10 nm to 70 nm, the thicknesses of the other layers are fixed, $FAPbI_3$ (750 nm) and *i*-SnO_2 (10 nm). The obtained results show that all the parameters of the cell are constant: $J_{SC} = 26.55$ mA/cm^2, $V_{OC} = 1.8$ V, FF = 82.79% and PCE = 26.07%. The thickness of the Cu_2O does not affect the performance of the cell.

Cell efficiency with Cu_2O is better compared to cells with Spiro-

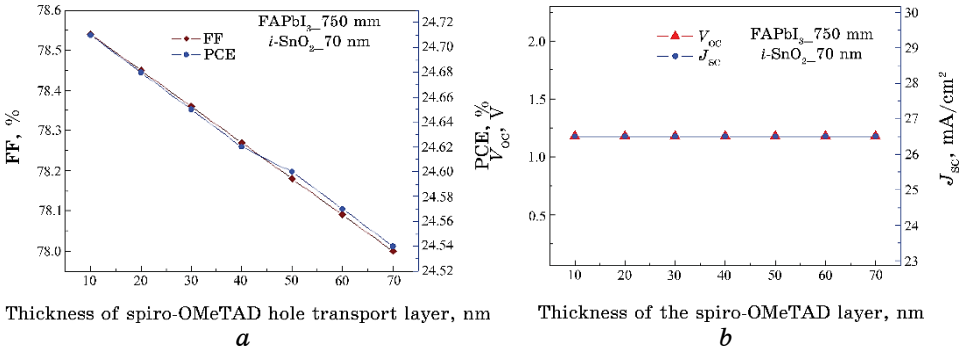

Fig. 3. Electrical parameters of the cell as function of the thickness of Spiro-OMeTAD. *a*) Fill factor and efficiency; *b*) open-circuit voltage and current density.

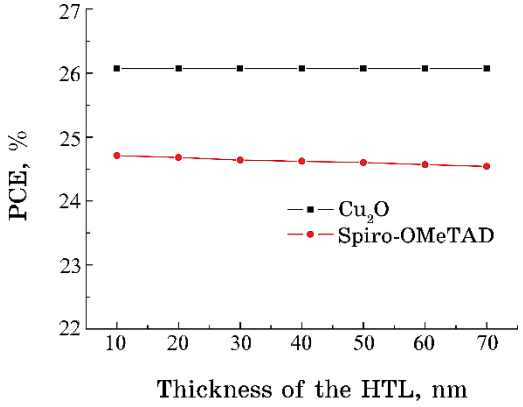

Fig. 4. Efficiency as function of the hole-transport layer.

OMeTAD, as illustrated in Fig. 4: $PCE_{(Cu_2O)} = 26.07\%$ and $PCE_{(Spiro\text{-}OMeTAD)} = 24.72\%$. The results show that efficiency does not affected by the thicknesses of the HTL, but the HTL type, as shown in Fig. 4, affects it.

3.3. Effect of the Electron-Transport Layers

3.3.1. Effect of the Thickness of *i*-SnO_2

The *i*-SnO_2 ETL has good properties such as excellent charge mobility, a low temperature preparation method, good transparency in the visible range, and a favourable energy level position that increases the efficiency of the perovskite solar cells. However, depositing SnO_2 film by spin-coating creates many pinholes and cracks in the film. The pinholes and cracks in the SnO_2 can results in direct contacts and carrier extraction losses between the perovskite absorber layer and electrode; leading to higher recombination losses and leakage current at the perovskite/hole-transport layer interface [14].

A small variation of PCE is observed when the thickness of *i*-SnO_2 increases from 10 nm to 70 nm. The fill factor increases as the thickness of *i*-SnO_2 increases, as shown in Fig. 5, *a*. The short-circuit current density remains constant as the thickness of the electron-transport layer (*i*-SnO_2) varies: $J_{SC} = 26.52$ mA/cm^2. The open-circuit voltage decreases as the thickness of *i*-SnO_2 increases, as shown in Fig. 5, *b*.

3.3.2. Effect of the Thickness of WS_2

Figure 6 shows efficiency of *i*-SnO_2-based solar cell compared to WS_2-based solar cell as function of thicknesses of the ETL. It is clear that structure based WS_2 exhibits better electrical parameters compared to that based *i*-SnO_2. WS_2 exhibits high carrier mobility, good conductivity in the order of 10^{-3} $\Omega^{-1}\cdot cm^{-1}$ and *n*-type semiconducting characteristics. WS_2 can be deposited through a solution process or by sputtering at low temperature [5].

The use of WS_2 as an electron-transport layer gives better performance compared to the use of *i*-SnO_2, as shown in Fig. 6. The yield obtained with 50 nm of WS_2 is 24.82%, while with *i*-SnO_2 the yield is 24.72%. Note that the HTL used in this case is Spiro-OMeTAD (10 nm) and $FAPbI_3$ (750 nm) as absorber layer.

3.4. Optimized Cell

From previous results, cells with Cu_2O used as HTL have better per-

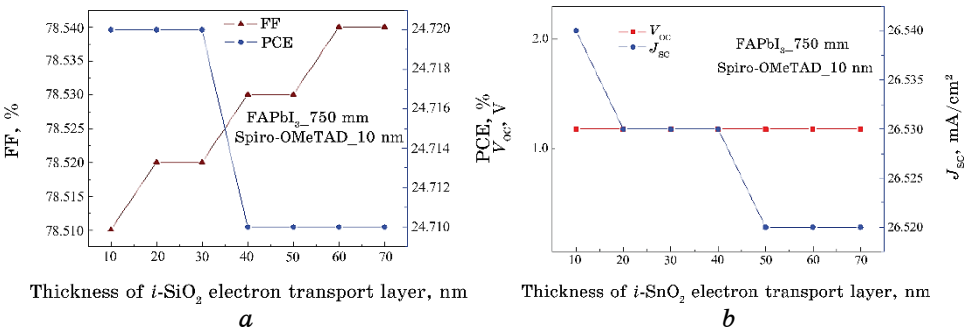

Fig. 5. Effect of the thickness of i-SnO_2 used as ETL on the performances of the perovskite cell. *a*) FF and PCE; *b*) V_{OC} and J_{SC}.

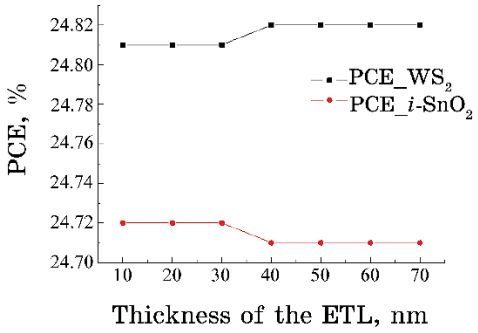

Fig. 6. Efficiency as function of the electron-transport layer obtained by simulation under SCAPS-1*D*.

formance than cells with Spiro-OMeTAD, and cells with WS_2 have better performance than cells with i-SnO_2. From these results, FTO/WS_2/$FAPbI_3$/Cu_2O/Au structure is simulated under SCAPS-1*D*. The best performance is obtained for cell with the following thicknesses of the layers: WS_2 (50 nm), $FAPbI_3$ (750 nm) and CuO_2 (10 nm). The obtained parameters are as follow: $V_{OC} = 1.18$ V, $J_{SC} = 26.57$ mA/cm^2, FF = 82.66% and PCE = 26.07%.

Figure 7 illustrates $J(V)$ characteristics of the optimized cell in the dark and under illumination.

3.5. Effect of the Defect of the Perovskite Layer on the Optimized Cell

Defect properties in absorber layer of solar cell play a critical role to determine the electron hole diffusion length and open circuit voltage. Deep level defects usually act as Shockley–Read–Hall non-radiative

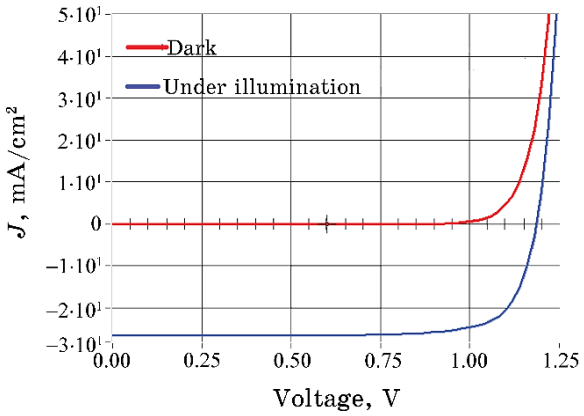

Fig. 7. $J(V)$ characteristics of the optimized cell in the dark and under illumination obtained by simulation under SCAPS software.

recombination centres. It is proved that these types of defects are responsible for short minority carrier lifetime, which results into lower V_{OC} in solar cells. More recently, the concept of amphoteric native defects has been used to control defect incorporation in compound semiconductors like $CH_3NH_3PbX_3$ in perovskite devices [15].

Simulation results show that cell performance decreases as the density of defects in $FAPbI_3$ increases, as shown in Fig. 8, *a*, *b*. The best efficiency is given for a defect concentration $1 \cdot 10^{10}/cm^3$. PCE is up to 36% because J_{SC} and V_{OC} are increased. PCE decreases, if the defect density in $FAPbI_3$ increased.

3.6. Effect of the Series Resistance

The variation of series resistance does not influence the variation of the short-circuit current density and the open-circuit voltage, $J_{SC} = 26.54$ mA/cm^2 and $V_{OC} = 1.8$ V, as shown by the curves of the $J(V)$ characteristics according to the series resistance in Fig. 9, *a*. PCE and FF decrease as the series resistance increases as shown in Fig. 9, *b*. The best performance is given for a low resistance. For $R_{serie} = 0$ Ohms/cm^2, PCE = 24.72%, and FF = 78.51%.

4. CONCLUSION

The use of cheap organometal halide perovskite materials, perovskite solar cells are a promising photovoltaic technology. Interfacial engineering strategy between the perovskite absorber and the charge transport layer play a vital role in highly efficient perov-

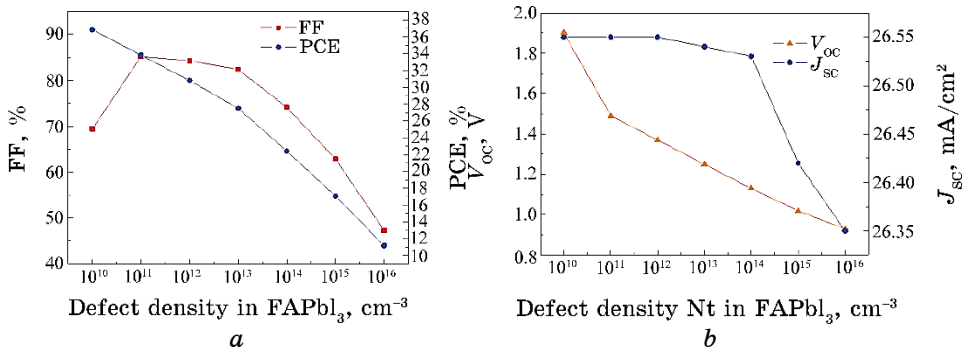

Fig. 8. Effect of the defect of the perovskite layer on cell performance. (*a*) PCE and FF; (*b*) V_{OC} and J_{SC}.

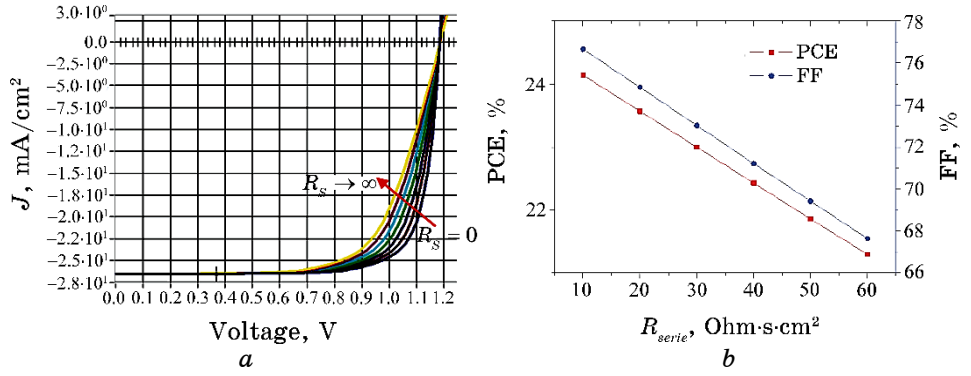

Fig. 9. Performance of the cell as function of the series resistance: (*a*) *J*(*V*) characteristics; (*b*) efficiency and fill factor.

skite solar cells. This study, allowed us to understand the role of certain parameters and different materials constituting the photovoltaic cell and their effects on efficiency. We have observed that the optimum thickness is located in the vicinity of 750 nm, which makes the thickness of the perovskite layer an interesting parameter to optimize while keeping the same configuration. The defects of the absorber layer, the series and shunt resistance are also influence the performance of the perovskite photovoltaic cells.

This study shows also that the use of inorganic materials as hole-transport layer such as Cu_2O gives better yields compared to cells with Spiro-OMeTAD. Likewise, the use of WS_2 as an electron transport layer gives a better yield compared to *i*-SnO_2. The results obtained show that a cell with WS_2 (50 nm), $FAPbI_3$ (750 nm) and Cu_2O (10 nm) gives an efficiency of 26.07%. Therefore, a highly

stable, non-toxic and environmentally friendly *n*-type semiconductor makes WS_2 a potential candidate as the ETL in $FAPbI_3$ perovskite solar cells. So, an in-depth study of FTO/WS_2/$FAPbI_3$/Cu_2O/Au structure is necessary to optimize the performance of this type of cell.

REFERENCES

1. A. A. Zhumekenov, M. I. Saidaminov, M. A. Haque, E. Alarousu, S. P. Sarmah, B. Murali, I. Dursun, X. H. Miao, A. L. Abdelhady, T. Wu, O. F. Mohammed, and O. M. Bakr, *ACS Energy Lett.*, **1**, No. 1: 32 (2016); https://doi.org/10.1021/acsenergylett.6b00002
2. W. S. Yang, J. H. Noh, N. J. Jeon, Y. C. Kim, S. Ryu, J. Seo, and S. I. Seok, *Science*, **348**, Iss. 6240: 1234 (2015); doi:10.1126/science.aaa92
3. N. Ahn, D. Y. Son, I. H. Jang, S. M. Kang, M. Choi, and N. G. Park, *J. Am. Chem. Soc.*, **137**, No. 27: 8696 (2015); https://doi.org/10.1021/jacs.5b04930
4. O. Ourahmoun, *Nanosistemi, Nanomateriali, Nanotehnologii*, **18**, No. 4: 1003 (2020); https://doi.org/10.15407/nnn.18.04.1003
5. K. Sobayel, Md. Akhtaruzzaman, K. S. Rahman, M. T. Ferdous, Zeyad A. Al-Mutairi, Hamad F. Alharbid, Nabeel H. Alharthie, Mohammad R. Karime, S. Hasmadyc, and N. Amin, *Results in Physics*, **12**: 1097 (2019); https://doi.org/10.1016/j.rinp.2018.12.049
6. A. Kumar and S. Singh, *Materials Today*, **26**, Part 2: 2574 (2020); https://doi.org/10.1016/j.matpr.2020.02.545
7. G. S. Chen, Y. C. Chen, C. T. Lee, and H. Y. Lee, *Solar Energy*, **174**: 897 (2018); https://doi.org/10.1016/j.solener.2018.09.078
8. A. Jena, A. Kulkarni, and T. Miyasaka, *Chemical Reviews*, **119**, No. 5: 3036 (2019); https://doi.org/10.1021/acs.chemrev.8b00539
9. Hasitha C. Weerasinghe, Yasmina Dkhissib, Andrew D. Scully, Rachel A. Caruso, and Yi-Bing Cheng, *Nano Energy*, **18**: 118 (2015); https://doi.org/10.1016/j.nanoen.2015.10.006
10. S. Song, B. J. Moon, M. T. Hörantner, J. Lim, G. Kang, M. Park, and T. Park, *Nano Energy*, **28**: 269 (2016); https://doi.org/10.1016/j.nanoen.2016.06.046
11. A. Suzuki, H. Okumura, Y. Yamasaki, and T. Oku, *Applied Surface Science*, **488**: 586 (2019); https://doi.org/10.1016/j.apsusc.2019.05.305
12. I. E. Tinedert, A. Saadoun, I. Bouchama, and M. A. Saeed, *Optical Materials*, **106**: 109970 (2020); https://doi.org/10.1016/j.optmat.2020.109970
13. L. Yang, U. B. Cappel, E. L. Unger, M. Karlsson, K. M. Karlsson, E. Gabrielsson, L. Sun, G. Boschloo, A. Hagfeldt, and E. M. J. Johansson, *Physical Chemistry Chemical Physics*, **14**: 779 (2012); https://doi.org/10.1039/C1CP23031J
14. Z. Hawash, L. K. Ono, S. R. Raga, M. V. Lee, and Y. Qi, *Chemistry of Materials*, **27**, No. 2: 562 (2015); https://doi.org/10.1021/cm504022q
15. K. Alberti and M. A. Scarpulla, *Scientific Reports*, **6**: 279 (2016); https://doi.org/10.1038/srep27954